Formation and Reactivity of (Octaethyltetraazaporphyrinato)rhodium Complexes

Yaping Ni, Jeffrey P. Fitzgerald, Patrick Carroll, and Bradford B. Wayland*

Departments of Chemistry, University of Pennsylvania, Philadelphia, Pennsylvania 19104-6323, and United States Naval Academy, Annapolis, Maryland 21402-5000

Received June 3, 1993®

A series of (octaethyltetraazaporphyrinato)rhodium, (OETAP)Rh, complexes including (OETAP)Rh–I, (OETAP)-Rh–CH_3, and $[(OETAP)Rh]_2$ were prepared for comparison with the corresponding (octaethylporphyrinato)-rhodium, (OEP)Rh, derivatives. $[(OETAP)Rh]_2$ (**1**) reacts like $[(OEP)Rh]_2$ (**2**) with CH_3I, CH_3NC, $(CH_3O)_3P$, and $CH_2{=}CH_2$ in forming (OETAP)Rh–CH_3 and (OETAP)Rh–I, (OETAP)Rh(CN)(CH_3NC), (OETAP)Rh–$P(O)(OCH_3)_2$, and (OETAP)Rh–CH_2CH_2–Rh(OETAP), respectively, but reactions of **1** are invariably much slower than those of **2**. $[(OETAP)Rh]_2$ fails to react with H_2, CO, CH_3CHO, and $CH_3C_6H_5$, which participate in prominent substrate reactions for **2**. Reactivity and equilibrium studies indicate that a substantially larger Rh–Rh bond dissociation enthalpy for **1** compared with **2** is primarily responsible for the slower rates and reduced scope of substrate reactions for $[(OETAP)Rh]_2$. Dissolution of **1** in pyridine results in formation of a persistent OETAP anion radical complex of Rh(III), $(OETAP^{\bullet-})Rh^{III}(py)_2$, which contrasts with **2** where disproportionation produces the $(OEP)Rh^{I}$ anion and the $(OEP)Rh^{III}(py)_2$ cation. (OETAP)Rh–CH_3 ($RhC_{33}H_{43}N_8$) crystallizes in the monoclinic system, space group $P2_1/c$, with a = 9.889(2) Å, b = 22.660(4) Å, c = 14.781(3) Å, β = 106.85(2)°, and Z = 4. The X-ray crystal and molecular structure determination for (OETAP)Rh–CH_3 reveals a smaller hole size and corresponding shorter Rh–N distances for the (OETAP)Rh derivative but virtually identical Rh–CH_3 bond distances in comparison with (OEP)Rh–CH_3. Differences in the structures and reactivities of (OETAP)Rh and (OEP)Rh complexes are discussed in terms of the smaller hole size, lower energy of the π^* orbitals, and the doming of the OETAP ligand.

Introduction

The (octaethylporphyrinato)rhodium(II) dimer, $[(OEP)Rh]_2$, and related rhodium(II) porphyrins manifest as unusual breadth of organometallic reactivity, which includes thermodynamically difficult processes such as formation of metalloformyl species from reactions of H_2 and CO,[1,2] CO reductive coupling,[3-5] and hydrocarbon activation.[6,7] This unusual scope of reactions results from the combination of weak Rh–Rh bonding and relatively strong Rh–C bonds whose energies can approach the values for Rh–H bonds (~60 kcal).[8-10] One of our continuing objectives has been to elaborate the ligand steric and electronic properties that contribute to the thermodynamic and kinetic parameters controlling this unusual reactivity.

Octaethyltetraazaporphyrin, $(OETAP)H_2$, where nitrogen is substituted for the bridging methine CH of porphyrin, is isoelectronic and structurally related with octaethylporphyrin, $(OEP)H_2$. Recent studies of the iron(II) and iron(III) derivatives

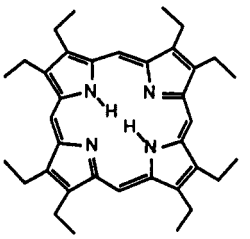

$(OEP)H_2$

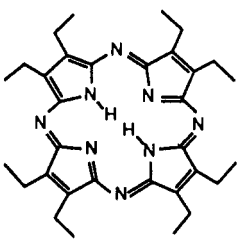

$(OETAP)H_2$

of OETAP indicate that the tetraazaporphyrin ligand is both a stronger σ donor and a more effective π acceptor than porphyrin ligands.[11,12] The larger d orbital separation associated with the enhanced ligand σ donor interaction produces an intermediate-spin state ($S = {}^3/_2$) for (OETAP)FeCl,[12] which contrasts with the high-spin state ($S = {}^5/_2$) observed for (OEP)FeCl.[13] Electronic differences in these complexes are also reflected in the substantially more favorable Fe(III)/Fe(II) reduction potentials for $(OETAP)Fe^{III}$ complexes compared with $(OEP)Fe^{III}$ derivatives.[12] Octaethyltraazaporphyrin and octaethylporphyrin provide a pair of ligands which are expected to have closely related structures and associated steric effects but substantially different electronic properties. This article reports the formation of rhodium complexes of OETAP and a comparative study of the reactivities of $[(OETAP)Rh]_2$ (**1**) and $[(OEP)Rh]_2$ (**2**).

Results and Discussion

(Octaethyltetraazaporphyrinato)rhodium iodide, (OETAP)-Rh–I (**3**), was prepared as a precursor to the methyl complex (OETAP)Rh–CH_3 (**4**) through BH_4^- reduction to the Rh^I anion $(OETAP)Rh^-$ and subsequent reaction with CH_3I. High-

* To whom correspondence should be addressed at the University of Pennsylvania.

® Abstract published in *Advance ACS Abstracts,* April 1, 1994.

(1) (a) Wayland, B. B.; Woods, B. A. *J. Chem. Soc., Chem. Commun.* **1981,** 700. (b) Wayland, B. B.; Woods, B. A.; Pierce, R. *J. Am. Chem. Soc.* **1982,** *104,* 302.
(2) (a) Wayland, B. B.; Duttaahmed, A.; Woods, B. A. *J. Chem. Soc., Chem. Commun.* **1983,** 142. (b) Wayland, B. B.; Van Voorhees, S. L.; Wilker, C. *Inorg. Chem.* **1986,** *25,* 4039.
(3) Wayland, B. B.; Sherry, A. E.; Poszmik, G.; Bunn, A. G. *J. Am. Chem. Soc.* **1992,** *114,* 1673.
(4) Coffin, V. L.; Brennen, W.; Wayland, B. B. *J. Am. Chem. Soc.* **1988,** *110,* 6063.
(5) (a) Wayland, B. B.; Sherry, A. E.; Coffin, V. L. *J. Chem. Soc., Chem. Commun.* **1989,** 662. (b) Wayland, B. B.; Woods, B. A.; Coffin, V. L. *Organometallics* **1986,** *5,* 1059.
(6) (a) Wayland, B. B.; Ba, S.; Sherry, A. E. *J. Am. Chem. Soc.* **1991,** *113,* 5305. (b) Sherry, A. E.; Wayland, B. B. *J. Am. Chem. Soc.* **1990,** *112,* 1259.
(7) Del Rossi, K. J.; Wayland, B. B. *J. Am. Chem. Soc.* **1985,** *107,* 7941.
(8) Wayland, B. B.; Coffin, V. L.; Farnos, M. D. *Inorg. Chem.* **1988,** *27,* 2745.
(9) Wayland, B. B. *Polyhedron* **1988,** *7,* 1545.
(10) Wayland, B. B. In *Energetics of Organometallic Species*; Simões, J., Ed.; Kluwer Academic Press: Dordrecht, The Netherlands, 1992; p 69.
(11) (a) Fitzgerald, J.; Taylor, W.; Owen, H. *Synthesis* **1991,** 686. (b) Cook, A.; Linstead, R. *J. Chem. Soc.* **1937,** 929.
(12) Fitzgerald, J. P.; Haggerty, B. S.; Rheingold, A. L.; May, L.; Brewer, G. A. *Inorg. Chem.* **1992,** *31,* 2006.
(13) Scheidt, W.; Reed, C. *Chem. Rev.* **1981,** *81,* 543.

0020-1669/94/1333-2029$04.50/0

Table 1. Crystallographic Data for (OETAP)Rh–CH_3[a]

formula	$RhC_{33}H_{43}N_8$	space group	$P2_1/c$ (No. 14)
fw	654.67	T	298 °C
a	9.889(2) Å	λ	1.541 84 Å
b	22.660(4) Å	D_{calc}	1.372 g/cm^3
c	14.781(3) Å	μ	47.07 cm^{-1}
β	106.85(2)°	R_1	0.049
V	3170(2) Å^3	R_2	0.055
Z	4		

[a] $R_1 = \Sigma||F_o| - |F_c||/\Sigma|F_o|$; $R_2 = (\Sigma w||F_o| - |F_c||^2/\Sigma w|F_o|^2)^{1/2}$; GOD = $(\Sigma w||F_o| - |F_c||^2/(N_O - N_V))^{1/2}$.

Table 2. Refined Positional Parameters for (OETAP)Rh–CH_3 and Their Estimated Standard Deviations[a]

atom	x	y	z	B_{eq}, Å^2
Rh	0.18574(4)	0.02271(2)	0.51721(3)	3.346(7)
N1	0.1415(5)	0.1068(2)	0.5198(3)	3.7(1)
N2	0.3213(5)	0.0302(2)	0.6438(3)	3.9(1)
N3	0.2292(4)	–0.0615(2)	0.5157(3)	3.56(9)
N4	0.0458(5)	0.0148(2)	0.3925(3)	3.7(1)
N5	0.3031(5)	0.1345(2)	0.6702(3)	4.5(1)
N6	0.4030(5)	–0.0708(2)	0.6683(3)	4.0(1)
N7	0.0837(5)	–0.0874(2)	0.3590(3)	3.8(1)
N8	–0.0250(5)	0.1171(2)	0.3641(3)	3.7(1)
C1	0.2039(6)	0.1456(3)	0.5897(4)	4.1(1)
C2	0.3559(6)	0.0811(3)	0.6940(4)	4.3(1)
C3	0.4687(7)	0.0684(3)	0.7815(4)	5.6(2)
C4	0.4952(7)	0.0095(3)	0.7816(4)	5.4(2)
C5	0.4028(6)	–0.0145(3)	0.6938(4)	4.2(1)
C6	0.3235(6)	–0.0922(3)	0.5862(4)	3.8(1)
C7	0.3289(6)	–0.1533(2)	0.5567(4)	4.0(1)
C8	0.2409(6)	–0.1579(2)	0.4677(4)	4.2(1)
C9	0.1765(6)	–0.0994(2)	0.4423(4)	3.7(1)
C10	0.0243(5)	–0.0345(2)	0.3361(4)	3.5(1)
C11	–0.0719(6)	–0.0197(3)	0.2436(4)	3.9(1)
C12	–0.1027(6)	0.0387(3)	0.2459(4)	3.9(1)
C13	–0.0263(5)	0.0606(2)	0.3383(4)	3.6(1)
C14	0.0514(6)	0.1378(2)	0.4476(4)	3.9(1)
C15	0.0546(6)	0.2002(3)	0.4743(4)	4.1(1)
C16	0.1475(6)	0.2050(2)	0.5614(4)	4.1(1)
C17	0.1922(7)	0.2586(3)	0.6209(5)	5.3(2)
C18	0.3203(9)	0.2875(4)	0.6094(6)	8.2(2)
C19	0.550(1)	0.1166(4)	0.8501(5)	9.3(3)
C20	0.490(1)	0.1254(5)	0.9230(9)	11.4(4)
C21	0.5993(9)	–0.0272(4)	0.8543(5)	7.0(2)
C22	0.722(1)	–0.0453(5)	0.8252(7)	9.3(3)
C23	0.4195(7)	–0.1995(3)	0.6171(5)	5.4(2)
C24	0.5677(8)	–0.2009(4)	0.6124(6)	7.4(2)
C25	0.2117(8)	–0.2094(3)	0.4038(5)	5.7(2)
C26	0.2965(9)	–0.2095(5)	0.3364(6)	10.7(3)
C27	–0.1209(7)	–0.0633(3)	0.1658(4)	5.0(2)
C28	–0.021(1)	–0.0722(4)	0.1077(5)	8.0(2)
C29	–0.1938(7)	0.0769(3)	0.1691(4)	4.9(1)
C30	–0.1121(9)	0.1126(4)	0.1186(6)	7.8(2)
C31	–0.0253(7)	0.2472(3)	0.4105(5)	5.0(2)
C32	0.0493(8)	0.2678(3)	0.3417(5)	6.8(2)
C33	0.3356(7)	0.0430(3)	0.4527(4)	4.9(1)

[a] $B_{eq} = {}^4/_3[\beta_{11}a^2 + \beta_{22}b^2 + \beta_{33}c^2 + \beta_{12}ab(\cos\gamma) + \beta_{13}ac(\cos\beta) + \beta_{23}bc(\cos\alpha)]$.

resolution FAB MS, electronic spectra, and ^{1}H NMR are used in characterizing these complexes in solution. The methyl complex, **4**, was further characterized by an X-ray crystal and molecular structure determination.

X-ray Crystal and Molecular Structures of (OETAP)Rh–CH_3. Crystals of (OETAP)Rh–CH_3 were obtained by slow evaporation of solvent from a chloroform/ethanol solution at room temperature. Crystal structure data, bond distances, and bond angles for (OETAP)Rh–CH_3 are given in Tables 1–3, and an ORTEP view is shown in Figure 1. The Rh–CH_3 distance in (OETAP)-Rh–CH_3 (2.034(7) Å) is indistinguishable from the value in (OEP)Rh–CH_3 (2.031(6) Å).[14] The average distances between

Table 3. Selected Bond Distances (Å) and Angles (deg) for (OETAP)Rh–CH_3

Bond Distances

Rh–N1	1.957(4)	N5–C1	1.328(7)	N7–C9	1.333(6)
Rh–N2	1.968(4)	N5–C2	1.324(8)	N7–C10	1.335(7)
Rh–N3	1.957(4)	N6–C5	1.331(8)	N8–C13	1.334(7)
Rh–N4	1.967(4)	N6–C6	1.331(6)	N8–C14	1.332(6)
Rh–C33	2.034(7)				

Bond Angles

N1–Rh–N2	89.5(2)	N3–Rh–N4	89.9(2)
N1–Rh–N3	179.4(2)	N3–Rh–C33	91.3(2)
N1–Rh–N4	90.3(2)	N4–Rh–C33	89.5(2)
N1–Rh–C33	89.2(2)	C1–N5–C2	122.9(5)
N2–Rh–N3	90.2(2)	C5–N6–C6	123.9(5)
N2–Rh–N4	178.3(2)	C9–N7–C10	123.5(5)
N2–Rh–C33	92.2(2)	C13–N8–C14	124.0(4)

the rhodium atom and pyrrolic nitrogen atoms (Rh–N) and between the pyrrolic α-carbon atoms and the bridging atoms (N or C–H) are smaller in the tetraazaporphyrin complex than in the porphyrin derivative. Also, the average bond angle about the bridging nitrogen atoms (C=N—C) in (OETAP)Rh–CH_3 (123.6(5)°) is smaller than the average angle about the bridging carbon atoms (C=CH—C) in (OEP)Rh–CH_3 (127.2(1)°).[14] Deviation of the Rh atom from the mean planes through the nitrogen donor atoms are 0.019 and 0.051 Å, respectively, in (OETAP)Rh–CH_3 and (OEP)Rh–CH_3.

Smaller bond distances and angles associated with the N bridging group (C–N = 1.33 Å, C–N–C = 124°) compared with the methine carbon bridge (C–C = 1.38 Å, C–CH–C = 127°) reduce the tetrapyrrole hole size for OETAP compared with OEP.[14] The distance between trans pyrrole nitrogens in OETAP is ~3.92 Å compared with ~4.06 Å in OEP. In spite of the smaller hole size, rhodium is found to be only 0.019 Å out of the mean pyrrole nitrogen plane in (OETAP)Rh–CH_3 compared with 0.051 Å for (OEP)Rh–CH_3. Placement of Rh in the plane of the pyrrole nitrogen donors of OETAP imposes substantially shorter Rh–N distances (1.96 Å) than those observed in (OEP)Rh–CH_3 (Rh–N = 2.03 Å). The relatively short Rh–N distances in (OETAP)Rh–CH_3 may be accommodated by partial multiple Rh–N bonding resulting from the $d\pi \rightarrow p\pi^*$ interaction. A lower energy position for the OETAP π^* orbital compared with that of OEP should produce more effective π bonding with the occupied rhodium $d_{xz,yz}$. The shorter Rh–N distances result in larger σ donor interactions that must elevate the $d_{x^2-y^2}$ and possibly the d_{z^2} orbital in (OETAP)Rh–CH_3 compared with (OEP)Rh–CH_3. Despite the substantial difference in Rh–N distances, the Rh–CH_3 distances are indistinguishable ((OETAP)Rh–CH_3 (2.034-(7) Å), (OEP)Rh–CH_3 (2.031 (6) Å)) and equal to the sum of covalent radii (1.26 + 0.77 = 2.03 Å). The small doming observed for the OETAP unit in both (OETAP)Rh–CH_3 and (OETAP)-Fe–Cl[12] may be a general structural feature of OETAP complexes.

Formation of [(OETAP)Rh]$_2$. Photolysis of (OETAP)Rh–CH_3 (**4**) in benzene ($\lambda > 350$ nm) results in formation of [(OETAP)Rh]$_2$ (**1**), which is identified by ^{1}H NMR (Figure 2b), electronic spectra (Figure 3), and high-resolution FAB MS (observed m/e 1278.479, calculated m/e for [(OETAP)Rh]$_2$ 1278.486). Electronic spectral changes that occur during the photolytic conversion of **4** to **1** in a spectrophotometric cell are illustrated in Figure 3. The series of isobestic points observed during the photolysis process indicates that a single absorbing species, [(OETAP)Rh]$_2$, is formed and that material balance associated with the quantitative conversion of **4** to **1** is effectively achieved. The broadening and splitting of the electronic spectrum of [(OETAP)Rh]$_2$ compared with **4** are similar to those observed for [(OEP)Rh]$_2$[15] and associated with π–π interactions that are

(14) Takenaka, A.; Syal, S. K.; Sasada, Y.; Omura, T.; Ogoshi, H.; Yoshida, Z. *Acta Crystallogr.* **1976**, *B32*.

(15) Setsune, J.; Yoshida, Z.; Ogoshi, H. *J. Chem. Soc., Perkin Trans. 1* **1982**, 983.

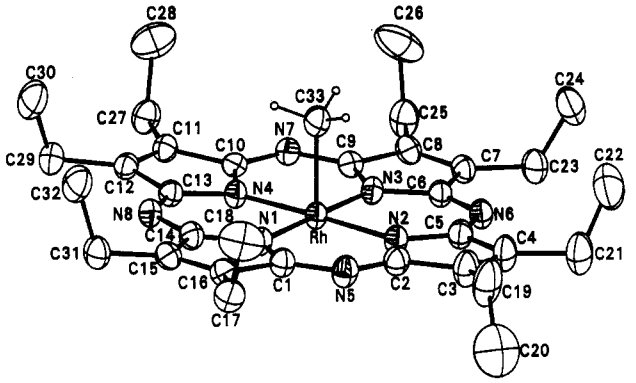

Figure 1. ORTEP view of (OETAP)Rh–CH_3 with thermal ellipsoids shown at the 50% probability level.

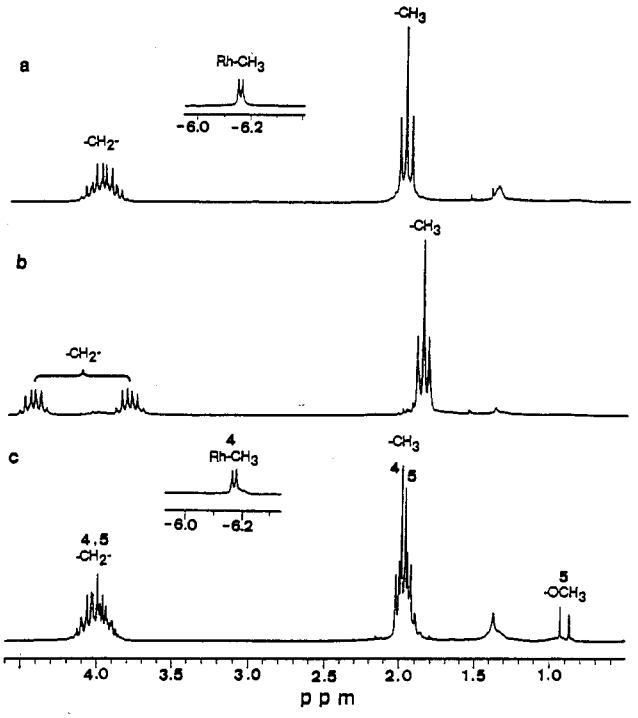

Figure 2. ^1H NMR (200 MHz) spectra in C_6D_6 (295 K) for (a) (OETAP)Rh–CH_3, (b) $[(OETAP)Rh]_2$, and (c) (OETAP)Rh–$P(O)(OCH_3)_2$ (**5**) and (OETAP)Rh–CH_3 (**4**) formed in the reaction of $[(OETAP)Rh]_2$ with $P(OCH_3)_3$ (1:1 ratio).

imposed in the cofacial dimer by the close approach required by Rh–Rh bonding.

^1H NMR of (OETAP)Rh–X Complexes. Replacement of the bridging methine group (=C(H)–) in OEP by nitrogen (=N–) in OETAP eliminates a valuable ^1H NMR structural probe. Identification of OETAP species in solution by ^1H NMR is limited to the use of the ethyl hydrogens. The ethyl CH_2 hydrogens are diastereotopic in (OETAP)Rh–X complexes where the macrocycle plane is not a molecular plane. Chemical shifts of the inequivalent (AB) CH_2 hydrogens are adequately sensitive to the nature of the group attached to rhodium to be used in distinguishing species in solution ((OETAP)Rh–X: X = I (δ_A = 4.11, δ_B = 3.93); X = CH_3 (δ_A = 4.05, δ_B = 3.92); X = (OETAP)Rh (δ_A = 4.43, δ_B = 3.80)). High-symmetry complexes in which the macrocycle plane is an effective molecular plane can also be identified by equivalence of the CH_2 hydrogens and their sensitivity to charge ($[(OETAP)Rh^I]^-$ (δ_{CH_2} = 3.68), $[(OETAP)Rh(py)_2]^+$ (δ_{CH_2} = 4.05)).

The ^1H NMR for the ethyl groups in $[(OETAP)Rh]_2$ (Figure 2b) is similar to that for $[(OEP)Rh]_2$ and highly characteristic of metal–metal-bonded dimers.[16] The difference in chemical shifts

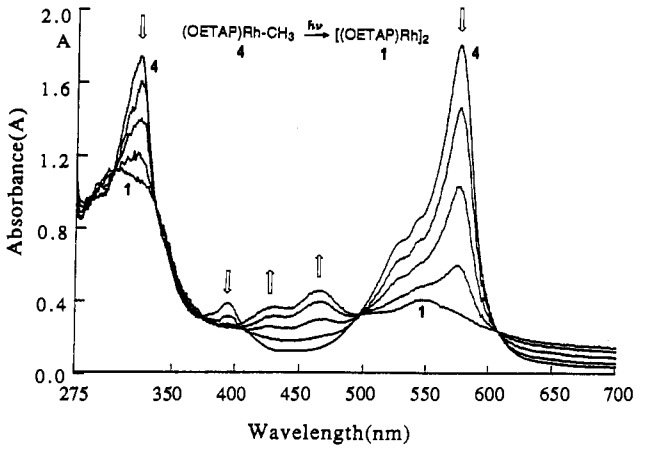

Figure 3. UV–visible spectral changes during the photolysis ($\lambda > 350$ nm) of (OETAP)Rh–CH_3 to form $[(OETAP)Rh]_2$ in benzene.

for the diastereotopic CH_2 hydrogens is particularly large for **1** and **2** because of the ring current of the adjacent cofacial aromatic macrocycle.

Ligands that are bonded with rhodium in (OETAP)Rh and (OEP)Rh complexes are situated at the center of the aromatic macrocycle ring current and are subject to large upfield NMR shifts. The ring current shift for the ^1H NMR is a valuable observable for identifying (OETAP)Rh–CH_3 (δ_{CH_3} = –6.16), (OETAP)Rh–CH_2CH_2–Rh(OETAP (δ_{CH_2} = –10.57), and (OETAP)Rh(CN)($CNCH_3$) (δ_{CNCH_3} = –1.48) and for comparison with the shifts for the corresponding (OEP)Rh derivatives ((OEP)Rh–CH_3 (δ_{CH_3} = –6.02), (OEP)Rh–CH_2CH_2–Rh(OEP) (δ_{CH_2} = –11.66), (OEP)Rh(CN)($CNCH_3$) (δ_{CNCH_3} = –1.76)).[17]

Reactions of $[(OETAP)Rh]_2$. The reactivities of $[(OETAP)Rh]_2$ (**1**) with a series of substrates were evaluated by observing the time evolution of the ^1H NMR for benzene solutions of the reactants in sealed NMR tubes protected from exposure to light. The (octaethyltetraazaporphyrinato)rhodium(II) dimer, $[(OETAP)Rh]_2$ (**1**), was observed to react with I_2, CH_3I, $P(OCH_3)_3$, CH_3NC, and $H_2C{=}CH_2$ in benzene (eqs 1–5) but not with H_2, CO, H_2/CO, CH_3CHO, and $CH_3C_6H_5$. Integration of the ^1H NMR for the reactants and products relative to a ^{13}C–*H* resonance in benzene demonstrated that material balance based on the OETAP ligand was obtained within the capability of ^1H NMR (~5%) for each of the substrate reactions.

$[(OETAP)Rh]_2$ (**1**) reacts rapidly and quantitatively with iodine in benzene to produce (OETAP)Rh–I (**3**) (eq 1).

$$[(OETAP)Rh]_2 + I_2 \rightarrow 2(OETAP)Rh\text{–}I \qquad (1)$$

Reaction of **1** with CH_3I in benzene yields (OETAP)Rh–I (**3**) and (OETAP)Rh–CH_3 (**4**) as the exclusive products (eq 2).The

$$[(OETAP)Rh]_2 + CH_3I \rightarrow (OETAP)Rh\text{–}CH_3 + (OETAP)Rh\text{–}I \qquad (2)$$

progress of reaction 2 is conveniently followed by appearance of the characteristic RhCH_3 ^1H NMR resonance at –6.16 ppm ($J_{^{103}Rh-H}$ = 2.9 Hz). Reaction 2 with a CH_3I to **1** molar ratio of 20 proceeds very slowly, requiring more than 1 month to reach completion at 295 K.

Trimethyl phosphite reacts with **1** in benzene to produce (OETAP)Rh–$P(O)(OCH_3)_2$ (**5**) and (OETAP)Rh–CH_3 (**4**) (eq 3). When the molar ratio of $P(OCH_3)_3$ to $[(OETAP)Rh]_2$ is 1 to 1, compounds **4** and **5** are formed in equal quantities, as shown

(16) (a) Collman, J. P.; Barnes, C. E.; Woo, L. K. *Proc. Natl. Acad. Sci. U.S.A.* **1983**, *80*, 7684. (b) Coffin, V. L.; Brennen, W.; Wayland, B. B. *J. Am. Chem. Soc.* **1988**, *110*, 6063.
(17) Poszmik, G.; Carroll, P. J.; Wayland, B. B. *Organometallics* **1993**, *12*, 3410.

$$[(OETAP)Rh]_2 + P(OCH_3)_3 \rightarrow (OETAP)Rh\text{–}CH_3 + (OETAP)Rh\text{–}P(O)(OCH_3)_2 \quad (3)$$

by the ^1H NMR (Figure 2c). (OETAP)Rh–P(O)$(OCH_3)_2$ (**5**) is identified in solution by the characteristic methyl doublet (δ = 0.90, $J_{^{31}POCH_3}$ = 12.0 Hz) (Figure 2c). In analogy with the reactions of trimethyl phosphite with $[(OEP)Rh]_2$[18] and (TMP)-$Rh^{II\bullet}$,[19] reaction 3 is envisioned as occurring through the intermediacy of a paramagnetic rhodium phosphite complex, $[(OETAP)Rh\text{–}P(OCH_3)_3]^\bullet$, which functions as a source of the methyl radical in reactions with **1** or $(OETAP)Rh^{II\bullet}$ in forming **4**. When a substantial excess of $P(OCH_3)_3$ is present ($P(OCH_3)_3$/(OETAP)Rh > 3), (OETAP)Rh–P(O)$(OCH_3)_2$ occurs in larger quantities than (OETAP)Rh–CH_3 because $P(OCH_3)_3$ completes with $(OETAP)Rh^{II}$ species for a methyl group in the intermediate to produce **5** and $[CH_3P(OCH_3)_3]^\bullet$, which catalyzes phosphite (P(III)) to phosphonate (P(V)) isomerization ($P(OCH_3)_3 \rightarrow CH_3P(O)(OCH_3)_2$).[18]

Reaction of CH_3NC (10^{-1} M) with **1** (10^{-3} M) in C_6D_6 (20 h, T = 333 K) produces equal quantities of (OETAP)Rh(CN)-($CNCH_3$) (**6**) and a rhodium methyl complex (eq 4). The

$$[(OETAP)Rh]_2 + 2CH_3NC \rightarrow (OETAP)Rh\text{–}CH_3 + (OETAP)Rh(CN)(CH_3NC) \quad (4)$$

coordinated methyl isocyanide group in the cyanide complex **6** is in limiting slow exchange with free ligand in solution and is directly observed by ^1H NMR as a high-field singlet (δ = –1.46). The methyl complex coordinates a methyl isocyanide ligand in solution, but coordinated and free isocyanides are in fast exchange such that evidence for the coordinated isocyanide is obtained only from the upfield shift of the Rh–CH_3 resonance (δ = –6.76) relative to its position in **4** (δ = –6.16). Removal of solvent and excess free ligand under vacuum and subsequent dissolution in C_6D_6 result in observation of the five-coordinate methyl complex (**4**) and the six-coordinate cyanide complex, (OETAP)Rh(CN)-(CH_3NC) (**6**). Cleavage of the CN–CH_3 bond and formation of an analogous set of complexes have also been observed for $[(OEP)Rh]_2$.[17]

Benzene solutions of **1** in contact with ethene ($P_{CH_2CH_2}$ = 200–700 Torr, T = 295 K) slowly reacts over a period of weeks to produce a two-carbon-alkanediyl-bridged complex, (OETAP)-Rh–CH_2CH_2–Rh(OETAP) (**7**) (eq 5). The bridging alkanediyl

$$[(OETAP)Rh]_2 + CH_2{=}CH_2 \rightleftharpoons (OETAP)Rh\text{—}CH_2CH_2\text{—}Rh(OETAP) \quad (5)$$

complex is identified in solution by ^1H NMR of the metal-bonded –CH_2CH_2– bridging unit and the $^{13}CH_2{}^{13}CH_2$ derivative (δ_{CH_2} = –10.57, $J_{^{13}C\text{–}H}$ = 142.6 Hz). Reaction 5 achieves an observable equilibrium at 295 K, and integrations of the ^1H NMR spectra for **1**, **7**, and ethene are used in evaluating the equilibrium constant for reaction 5 (K_5(295 K) ~ 130 ± 30; $\Delta G_5°$(295 K) ~ –2.9 ± 0.1 kcal mol^{-1}).

Benzene solutions of **1** (10^{-3} M) pressurized with H_2 (200 Torr, 290–350 K), CO (0.5–5 atm, 295 K), and H_2/CO (0.31 atm of H_2, 0.48 atm of CO, 295 K), respectively, did not produce any observed reactions over a period of several months under the specified conditions. Benzene solutions of **1** also failed to react with CH_3CHO (100 molar excess, T = 295–350 K) and $CH_3C_6H_5$ (100 molar excess, T = 295–350 K) over a period of 1 month.

Reaction of [(OETAP)Rh]$_2$ with Pyridine. Dissolution of $[(OETAP)Rh]_2$ (**1**) in deuterated pyridine results in a new species (**8**) with the ^1H NMR spectrum shown in Figure 4 and electronic spectrum shown in Figure 5. The species formed in pyridine solution (**8**) displays a large downfield shift for the CH_2 resonance (δCH_2 = 28.8; T = 295 K) with an inverse temperature dependence (Figure 4) indicative of Curie paramagnetic behavior. Positive spin density at the methylene hydrogens associated with the downfield shift is interpreted as resulting from a hyperconjugative interaction of the CH_2 hydrogens with a partially occupied ligand π^* orbital. Relatively large contributions from the pyrrole β-carbon pπ orbitals to the LUMO (e_g) of tetraazaporphyrin species support this interpretation.[20] The electronic spectrum for **8** (Figure 5) is substantially changed from those of other (OETAP)Rh complexes, suggesting disruption of the ligand π system and appearance of a low-energy transition (λ = 750 nm) that in analogy with porphyrins is suggestive of a ligand π radical.[21] Frozen solutions (90 K) of **8** in pyridine show an intense relatively broad (90 MHz) EPR signal centered at g = 1.998, compatible with a ligand-based radical species.[22] The EPR spectrum and the pattern of ^1H NMR contact shifts are consistent with placing the unpaired electron in the aromatic ligand π^* orbitals. Observation of g values close to that for the free electron (g_e = 2.0023) is not compatible with significant rhodium d orbital spin

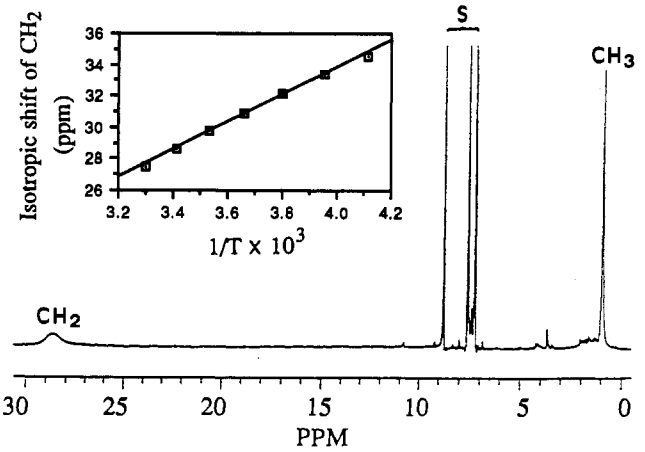

Figure 4. ^1H NMR (200 MHz) spectrum of a solution prepared by dissolving $[(OETAP)Rh]_2$ in pyridine-d_5 at 295 K and an insert showing the temperature dependence for the CH_2 resonances.

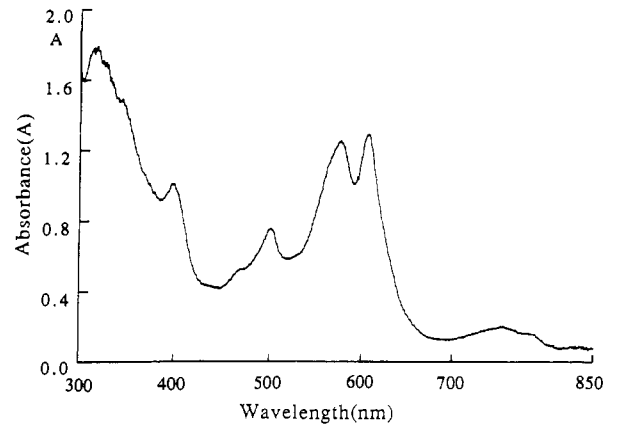

Figure 5. Electronic spectrum of a solution resulting from dissolving $[(OETAP)Rh]_2$ in pyridine at 295 K.

(18) Wayland, B. B.; Woods, B. A. *J. Chem. Soc., Chem. Commun.* **1981**, 475.
(19) Wayland, B. B.; Sherry, A. E.; Bunn, A. G. *J. Am. Chem. Soc.* **1993**, *115*, 7675.
(20) (a) Weiss, C.; Kobayashi, H.; Gouterman, M. *J. Mol. Spectrosc.* **1965**, *16*, 415. (b) Schaffer, A.; Gouterman, M.; Davidson, E. *Theor. Chim. Acta* **1973**, *30*, 9.
(21) (a) Closs, G. L.; Closs, L. E. *J. Am. Chem. Soc.* **1963**, *85*, 818. (b) Stolzenberg, A. M.; Stershic, M. T. *J. Am. Chem. Soc.* **1988**, *110*, 6391. (c) Kadish, K. M.; Sazou, D.; Maiya, G. B.; Han, B. C.; Lin, Y. M.; Saoiabi, A.; Ferhat, M.; Guilard, R. *Inorg. Chem.* **1989**, *28*, 2542. (d) Fuhrhop, J. H.; Mauzerall, D. *J. Am. Chem. Soc.* **1969**, *91*, 4174.
(22) (a) Seth, J.; Bocian, D. F. *J. Am. Chem. Soc.* **1994**, *116*, 143. (b) Felton, R. H.; Limschitz, H. *J. Am. Chem. Soc.* **1966**, *88*, 1113.

density, which would introduce orbital angular momentum into the ground state through spin–orbit coupling.[23] Low-spin d^7 complexes where the odd electron occupies a $d\pi$ (d_{xz}^1 or d_{yz}^1) orbital have large deviations from the free-electron g value, as illustrated by (Salen)Co^{II}, where the $(d_{xy}d_{z^2}dx_z)^6d_{yz}^1$ configuration gives rise to $g_{xx} = 3.80$, $g_{yy} = 1.66$, and $g_{zz} = 1.74$.[24] Compound **8** is thus assigned as a π anion radical complex of Rh^{III}, $(OETAP^{\bullet-})Rh(py)_n$. Dissolving **1** in NC_5H_5, removal of excess pyridine under vacuum, and then dissolution of the product (**8**) in C_6D_6 result in reappearance of the electronic spectrum for $[(OETAP)Rh]_2$ (**1**) and an ^1H NMR spectrum showing that **8** converts back to NC_5H_5 and **1** in a molar ratio of 3.8 ± 0.2. These spectroscopic results in conjunction with the FAB MS for the NC_5D_5 adduct (m/e 807) establish **8** as a π anion radical complex with the formula $(OETAP)Rh(NC_5H_5)_2$ (eq 6). Reaction 6 is

$$[(OETAP)Rh]_2 + 4NC_5H_5 \overset{py}{\rightleftharpoons} 2(OETAP)Rh(NC_5H_5)_2 \quad (6)$$

envisioned as occurring through adduct formation of pyridine with $[(OETAP)Rh]_2$, which reduces the Rh–Rh homolysis enthalpy, forming $(OETAP)Rh{\cdot}NC_5H_5$, and subsequent interaction with a second pyridine raises the d_{z^2} MO above the π^* orbital (see diagram), resulting in donor-induced intramolecular electron

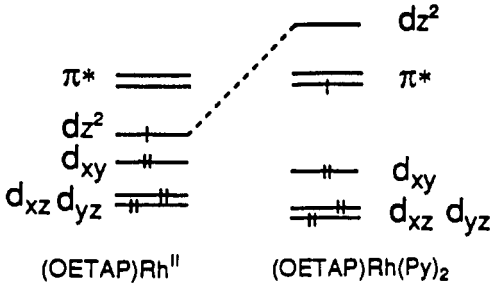

transfer from Rh^{II} to the (OETAP) π^* (e_g) orbital (eqs 7–9).

$$[(OETAP)Rh]_2 + py \rightleftharpoons [(OETAP)Rh]_2py \quad (7)$$

$$[(OETAP)Rh]_2py + py \rightleftharpoons 2(OETAP)Rh{\cdot}py \quad (8)$$

$$(OETAP)Rh{\cdot}py + py \rightleftharpoons [(OETAP)Rh(py)_2]^{\bullet} \quad (9)$$

Ligand-induced intramolecular oxidation of Rh^{II} is thermodynamically justified by the enhanced binding of Rh^{III} with pyridine. The unusual feature of this reaction is the reversible formation of a persistent anion radical complex. A closely related series of reactions is observed for $[(OEP)Rh]_2$[25] and $(TMP)Rh^{\bullet}$ [19] with pyridine except that the anion radical species $(por^{\bullet-})Rh(py)_2$ is proposed as an intermediate that disproportionates into diamagnetic $[(por)Rh^{I}]^-$ anionic and $[(por)Rh^{III}(py)_2]^+$ cationic species.[19,25] The lower energy position for the π^* orbital of OETAP compared with OEP apparently stabilizes the rhodium(III) anion radical complex, $(OETAP^{\bullet-})Rh(py)_2$, relative to the (OEP)Rh system.

Comparative Reactivity Studies of $[(OETAP)Rh]_2$ and $[(OEP)Rh]_2$. The (octaethylporphyrinato)rhodium(II) dimer, $[(OEP)Rh]_2$ (**2**), reacts with a wide range of substrates, including H_2, H_2/CO, CO, CH_3CHO, $CH_3C_6H_5$, CH_3I, CH_3NC, and $P(OCH_3)_3$.[1-8] The relatively small dissociation enthalpy for $[(OEP)Rh]_2$ (~16 kcal mol^{-1})[8,9] provides only a moderate thermodynamic barrier for substrate reactions and makes $[(OEP)Rh]_2$ a good source of the metalloradical monomer $((OEP)Rh^{\bullet})$ in hydrocarbon media. The wide range of thermodynamically favorable organometallic reactions of $[(OEP)Rh]_2$ results from formation of relatively strong (OEP)Rh–C ((OEP)Rh–CHO (~59 kcal mol^{-1}, (OEP)Rh–CH_3 (~58 kcal mol^{-1}), (OEP)Rh–CH_2R (~50 kcal mol^{-1})) and (OEP)Rh–H (~62 kcal mol^{-1}) bonds.[8-10].

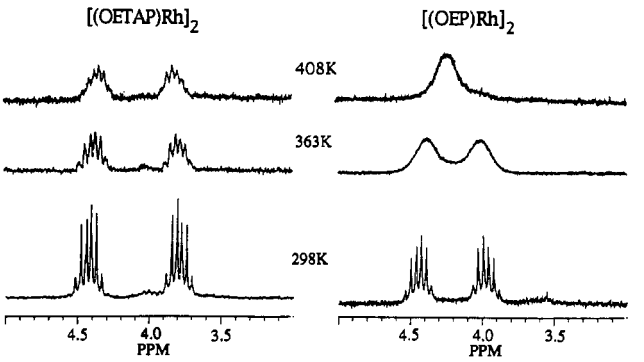

Figure 6. Comparison of the line broadening of the CH_2 hydrogen peaks with increasing temperature as seen in the ^1H NMR (200 MHz) spectrum of a benzene-d_6 solution of $[(OETAP)Rh]_2$ and $[(OEP)Rh]_2$.

$[(OETAP)Rh]_2$ reacts with CH_3I, CH_3NC, $P(OCH_3)_3$, and $CH_2{=}CH_2$ (eqs 2–5) in a manner that parallels the reactions of $[(OEP)Rh]_2$, but with relative rates that are several orders of magnitude slower. No reactions were observed for $[(OETAP)Rh]_2$ with H_2, CO, H_2/CO, CH_3CHO, and $CH_3C_6H_5$, which are substrates that readily react with $[(OEP)Rh]_2$. The slower rates observed for reactions of $[(OETAP)Rh]_2$ (**1**) compared with $[(OEP)Rh]_2$ (**2**) suggest that the activation enthalpy for Rh–Rh bond homolysis is substantially larger for **1** than for **2**, and the smaller scope of organometallic reactions for **1** further suggests that a larger bond homolysis enthalpy for **1** is not compensated by corresonding increases in the (OETAP)Rh–C and (OETAP)Rh–H bond dissociation enthalpies compared with the values for (OEP)Rh derivatives.

The activation enthalpy for dissociation of $[(OEP)Rh]_2$ (ΔH^* ~ 18.5 kcal mol^{-1}) and bond dissociation enthalpy (~16 kcal mol^{-1}) have been estimated from the ^1H NMR line broadening associated with exchange of the diamagnetic dimer with the paramagnetic monomer.[8] The ^1H NMR for $[(OETAP)Rh]_2$ is not significantly broadened or shifted in the convenient temperature range (295–408 K) where the ^1H NMR for $[(OEP)Rh]_2$ manifests substantial exchange broadening and merging of the diastereotopic CH_2 hydrogens (Figure 6). Absence of ^1H NMR line broadening for **1** is consistent with $[(OETAP)Rh]_2$ having a significantly slower rate of dissociation and larger enthalpy of dissociation than $[(OEP)Rh]_2$. The absence of significant line broadening or shifts at 408 K places an upper limit on the rate constant (k_f) and a lower limit on the ΔG^* for dissociation of $[(OETAP)Rh]_2$ (k_f(408 K) < 5 s^{-1}; ΔG^*(408 K) > 23 kcal mol^{-1}), which infers that the activation enthalpy for dissociation (ΔH^*) for $[(OETAP)Rh]_2$ must be more than 5 kcal mol^{-1} larger than the value for $[(OEP)Rh]_2$.

Reactions of **1** and **2** with ethene to form two-carbon-alkanediyl-bridged ($Rh–CH_2CH_2–Rh$) complexes provide the only opportunity for comparison of successful organometallic reactivities. The reaction of $[(OEP)Rh]_2$ with ethene to form (OEP)Rh–CH_2CH_2–Rh(OEP) effectively proceeds to completion such that the equilibrium constant could not be evaluated by ^1H NMR, which implies that the enthalpy change is greater than 20 kcal mol^{-1},[26] but $[(OETAP)Rh]_2$ reacts with ethene to produce an observable equilibrium with the two-carbon-alkanediyl-bridged complex (OETAP)Rh–CH_2CH_2–Rh(OETAP) (eq 5). Equilibrium studies for reaction 5 yield K_5(298 K) ~ 130 ± 30 ($\Delta G_5°$-

(23) McGarvey, B. R. *Can. J. Chem.* **1975**, *53*, 2498.
(24) Zelewsky, A.; Fierz, H. *Helv. Chim. Acta* **1973**, *56*, 977.
(25) Wayland, B. B.; Balkus, K. J.; Farnos, M. D. *Organometallics* **1989**, *8*, 950.
(26) Wayland, B. B.; Feng, Y.; Ba, S. *Organometallics* **1989**, *8*, 1438.

(298 K) ~ 2.9 ± 0.1 kcal mol^{-1}), and assuming $\Delta S_5° \sim -25$ cal K^{-1} mol^{-1} places $\Delta H_5°$ at approximately −10 kcal mol^{-1}, which indicates reaction 5 is more than 10 kcal mol^{-1} less enthalpy favorable than the corresponding $[(OEP)Rh]_2$ reaction. A large fraction of the enthalpy difference in reactions of ethene with **1** and **2** must result from the larger dissociation enthalpy of $[(OETAP)Rh]_2$ compared with **2**.

A larger dissociation enthalpy for $[(OETAP)Rh]_2$ (**1**) compared with $[(OEP)Rh]_2$ (**2**) could result from either a lower energy for **1** relative to **2** or a higher energy of (OETAP)Rh• compared with (OEP)Rh• or both. Rhodium occupies a position in or near the plane of the pyrrole nitrogen donors in the monomer metalloradicals, but dimerization by Rh–Rh bonding necessitates movement of rhodium out of plane (~0.15–0.20 Å) because the distance of closest approach for the aromatic macrocycles planes (~3.2–3.3 Å) corresponds to a nonbonding Rh–Rh distance. The σ and π bondings of rhodium with the macrocycle are maximized when the metal is in the macrocycle plane, and thus dimerization decreases the Rh–macrocycle bonding. A smaller hole size and lower energy π^* associated with the OETAP ligand produce more effective σ and π bondings with rhodium than those of the OEP ligand, which should stabilize (OETAP)Rh• relative to the dimer **1** more than in the (OEP)Rh system. The rhodium–macrocycle bonding effects should produce a smaller dissociation enthalpy for **1** compared to **2**, which is inconsistent with experiment. This argument points to differences in the interactions present in the dimers (**1**, **2**) as the origin for the larger dissociation enthalpy for $[(OETAP)Rh]_2$. Superior π acceptor properties of OETAP may reduce the repulsive interactions between the filled $d\pi$ orbitals of adjacent rhodium centers and provide an electronic effect that increases the effective Rh–Rh bond enthalpy in **1** relative to **2**. Also, the original premise that differences in the steric demands of OETAP and OEP are negligible may need to be revised. Substitution of N for CH contracts the hole and ring size and produces a small doming of the macrocycle. Subtle differences in the large number of interatomic contacts at the peripheries of $[(OETAP)Rh]_2$ and $[(OEP)Rh]_2$ may prove to be important. Resolution of this issue must await detailed structural and theoretical analysis. Further extension of the unusual organometallic reactivity of rhodium(II) porphyrins to tetraazaporphyrin analogs will require introducing more sterically demanding substituents that reduce the Rh–Rh bond dissociation enthalpy.

Experimental Section

General Methods. All manipulations were performed under nitrogen or by vacuum-line techniques. Proton NMR spectra were obtained on a Bruker WP200SY interfaced to an Aspect 300 computer. Electronic spectra were obtained through the use of a Hewlett-Packard UV 8452 instrument interfaced to an IBM PC. Electron paramagnetic resonance spectra were obtained by use of an EPR 100D X-band spectrometer. Mass spectrometry results were obtained on a VG ZAB-E mass spectrometer using the fast-atom-bombardment (FAB) method. Photolysis experiments were performed in a circular Rayonet photochemical reactor (New England Photochemical Co.) equipped with 16 RPR-3500A tubes.

Solvents. Benzene-d_6 and benzene used as solvents for NMR and electronic spectral studies were first degassed by freeze–pump–thaw cycles, refluxed over sodium/benzophenone until the indicator turned purple, and then degassed again. Chloroform used in the synthesis of (OETAP)Rh–I was washed three times with water and then dried by passing through a grade 1 neutral alumina column. Pyridine and pyridine-d_5 were dried with calcium hydride, distilled under vacuum, and stored over molecular sieves (4 Å).

Reagents. Octaethyltetraazaporphyrin, $(OETAP)H_2$, was prepared by a previously published procedure.[11a] Methyl isocyanide was prepared by the method of Weber and Ugi[27] and stored over Type 4A molecular sieves to remove water. Ethene (CP grade) was purchased from Matheson. All other reagents were purchased from Aldrich.

Synthesis and Characterization. (OETAP)Rh–I. To a two-neck flask fitted with an addition funnel and containing a solution of 100 mg of $(OETAP)H_2$ in 50 mL of dry chloroform was added dropwise under nitrogen 100 mg of $[Rh(CO)_2Cl]_2$ dissolved in 15 mL of dry chloroform. The resulting mixture was then stirred under nitrogen at room temperature. After 3 days, no unmetalated tetraazaporphyrin was present, as monitored by UV–visible spectroscopy. Iodine (80 mg) was then added to the solution in two stages, 60 mg initially and an additional 20 mg after 2 h. The reaction mixture was then stirred at room temperature for an additional 6 h. The crude product was concentrated by rotary evaporation after washing with saturated $Na_2S_2O_3$ solution twice and chromatographed on grade 3 neutral alumina using chloroform as the eluent to give (OETAP)Rh–I with an isolated yield of 70% based on $(OETAP)H_2$. (OETAP)Rh–I: UV–visible (C_6H_6) λ_{max} = 346, 534, 584 nm; ^{1}H NMR (C_6D_6) δ = 4.11 (–CH_2–, m, 8H), 3.93 (–CH_2–, m, 8H), 1.98 (–CH_3, t, 24H); HR FAB MS m/e = 766.153 (calculated for (OETAP)Rh–I m/e = 766.148).

(OETAP)Rh–CH_3. Absolute ethanol (25 mL) and (OETAP)Rh–I (25 mg) were mixed, and the resulting solution was filtered. The filtrate was flushed with nitrogen for 60 min. $NaBH_4$ (7 mg) in 2 mL of aqueous 0.5 M NaOH was added to the solution under nitrogen, and the resulting solution was then stirred for 8 h. Addition of 0.1 mL of CH_3I resulted in formation of a purple precipitate, which was collected by filtration. The precipitate was dissolved in benzene, and the mixture was filtered to remove the inorganic salts. The filtrate was chromatographed on grade 3 neutral alumina, and (OETAP)Rh–CH_3 was then isolated in 80% yield based on (OETAP)Rh–I by evaporation of the solvent. (OETAP)Rh–CH_3: UV–visible (C_6H_6) λ_{max} = 323, 393, 528, 543, 576 nm; ^{1}H NMR (C_6D_6) δ = 4.05 (–CH_2–, m, 8H), 3.92 (–CH_2–, m, 8H), 1.98 (–CH_3, t, 24H), –6.16 (Rh–CH_3, d, 3H), $J_{^{103}Rh-H}$ = 2.9 Hz; HR FAB MS m/e = 654.265 (calculated for (OETAP)Rh–CH_3 m/e = 654.267).

$[(OETAP)Rh]_2$. $[(OETAP)Rh]_2$ was prepared by photolysis of benzene solutions of (OETAP)Rh–CH_3 in vacuum-adapted NMR tubes or spectrophotometric cells. A degassed benzene solution of (OETAP)Rh–CH_3 (1 mg/0.5 mL) in a vacuum-adapted NMR tube was photolyzed ($\lambda > 350$ nm) for 10 h in a Rayonet photoreactor. The benzene solvent and the methane and toluene reaction products were removed under vacuum. $[(OETAP)Rh]_2$: UV–visible (C_6H_6) λ_{max} = 306, 430, 466, 548 nm; ^{1}H NMR (C_6D_6) δ = 4.43 (–CH_2–, m, 16H), 3.80 (–CH_2–, m, 16H), 1.87 (–CH_3, t, 48 H); HR FAB MS m/e = 1278.479 (calculated for $[(OETAP)Rh]_2$ m/e = 1278.486).

(OETAP)Rh$^-$. The (OETAP)Rh$^-$ anion was generated in NMR tubes for the purpose of obtaining ^{1}H NMR and UV–vis spectral parameters. A 0.5-mL ethanol solution of (OETAP)Rh–I (1 mg) and a 0.3-mL 0.5 N NaOH solution containing 0.3 mg of $NaBH_4$ were placed respectively into two interconnected NMR tubes which were attached to a vacuum-adapted stopcock. The two solutions were degassed by three freeze–pump–thaw cycles and then decanted into one NMR tube under vacuum. After a period of 10 h, the solvents were pumpsed out and C_6D_6 was vacuum-distilled into the NMR tube, which was then sealed off to record the ^{1}H NMR spectrum. The UV–vis spectrum was obtained by transferring the (OETAP)Rh$^-$/benzene solution into a vacuum-adapted UV–vis cell and diluting with C_6H_6 under argon in an inert-atmosphere box. Spectral data: ^{1}H NMR (C_6D_6) δ = 3.68 (q, 16H, –CH_2–), 1.90 (t, 24H, –CH_3); UV–vis (C_6H_6) λ_{max} = 388, 458, 518, 562 nm.

Attempts to form (OETAP)Rh–H by protonation of the Rh^I complex, (OETAP)Rh$^-$, invariably resulted in producing $[(OETAP)Rh]_2$, presumably through rapid bimolecular reductive elimination of H_2 (2(OETAP)Rh–H → $[(OETAP)Rh]_2 + H_2$).

Reactions of $[(OETAP)Rh]_2$. Substrate reactions of $[(OETAP)Rh]_2$ were carried out in sealed NMR tubes that were protected from light. $[(OETAP)Rh]_2$ was generated in vacuum-adapted NMR tubes by photolysis (10 h, $\lambda \geq 350$ nm) of (OETAP)Rh–CH_3 (1 mg/0.5 mL) in C_6H_6. The solution was then evacuated to dryness to remove the volatile photolysis products (CH_4 and $CH_3C_6H_5$) and C_6H_6 solvent. Subsequent additions of C_6D_6 (0.5 mL) solvent and substrates by vacuum-transfer were made, and the NMR tubes were then sealed and wrapped with aluminum foil to protect the samples from exposure to laboratory light. Progress of the substrate reactions was followed by observing the ^{1}H NMR immediately following preparation of the solution and at a series of time intervals. Integration of the ^{1}H NMR for the (OETAP)Rh species relative to a ^{13}C–H resonance of benzene solvent was used in monitoring the material balance associated with the initial reactant ([(OETAP)-

(27) Weber, W. P.; Gokel, G. W.; Ugi, I. K. *Angew. Chem., Int. Ed. Engl.* **1972**, *11*, 530.

$Rh]_2$) and the products containing the (OETAP)Rh fragment. Material balance of (OETAP)Rh units was obtained for each of the substrate reactions within ~5%.

I_2. Iodine (~0.4 mg) was vacuum-transferred to an NMR tube containing a C_6D_6 solution of $[(OETAP)Rh]_2$ (1 mg/0.5 mL). The tube was sealed and the ^1H NMR spectrum recorded. $[(OETAP)Rh]_2$ was observed to be quantitatively converted to (OETAP)Rh–I within the time required to record the spectrum. (OETAP)Rh–I was identified in solution by comparison of the ^1H NMR parameters with the spectrum obtained for authentic samples prepared by direct synthesis.

CH_3I. Methyl iodide (~2 mg) was vacuum-transferred to a vacuum-adapted NMR tube containing C_6D_6 solutions of $[(OETAP)Rh]_2$ (1 mg/0.5 mL). The NMR tube was sealed, and ^1H NMR was used to follow the evolution of products. A slow reaction resulted in formation of equal quantities of (OETAP)Rh–I and (OETAP)Rh–CH_3, as measured by integration of the ^1H NMR. $[(OETAP)Rh]_2$ was completely consumed only after a period of 3 months at room temperature.

CH_3NC. Methyl isocyanide was vacuum-transferred to vacuum-adapted NMR tubes containing C_6D_6 solutions of $[(OETAP)Rh]_2$ (1 mg/0.5 mL). The NMR tube was sealed, and ^1H NMR was used in following the reaction, which yielded (OETAP)Rh(CH_3)(CH_3NC) and (OETAP)Rh(CN)(CH_3NC) in equal amounts within a period of 1 day at 60 °C. Excess isocyanide in solution coordinated the sixth coordination site of the rhodium methyl complex, causing an upfield shift of the axial methyl hydrogen resonance relative to the position for the five-coordinate complex. The coordinated ligand was in fast exchange with uncoordinated isocyanide in case of (OETAP)Rh(CH_3)(CH_3NC) and in slow exchange in case of (OETAP)Rh(CN)(CH_3NC). (OETAP)Rh(CH_3)CH_3NC): ^1H NMR (C_6D_6) δ = 3.99 (m, 16H, $-CH_2-$), 2.01 (t, 24H, $-CH_3$), –6.76 (d, 3H, Rh–CH_3, $^2J_{Rh-H}$ = 2.4 Hz). (OETAP)Rh(CN)(CH_3NC): ^1H NMR (C_6D_6) δ = 4.00 (m, 16H, $-CH_2-$), 1.98 (t, 24H, $-CH_3$), –1.46 (s, 3H, $CNCH_3$); IR (KBr) ν(C≡N) = 2255, 2191 cm^{-1}.

$P(OCH_3)_3$. Variable quantities of trimethyl phosphite were vacuum-transferred to vacuum-adapted NMR tubes containing C_6D_6 solutions of $[(OETAP)Rh]_2$ (1 mg/0.5 mL). The NMR tubes were sealed, and ^1H NMR was used to follow the reactions (T = 295 K). When the molar ratio of $P(OCH_3)_3$ to $[(OETAP)Rh]_2$ was 1 to 1, this reaction yielded (OETAP)Rh–CH_3 and (OETAP)Rh–P(O)(OCH_3)$_2$ in equal amounts as exclusive products within a period of 1 day. When an excess of $P(OCH_3)_3$ was present, (OETAP)Rh–P(O)(OCH_3)$_2$ formed in larger quantity than (OETAP)Rh–CH_3. The excess trimethyl phosphite coordinated into the sixth coordination site of (OETAP)Rh–CH_3, causing an upfield shift of the axial methyl hydrogen resonance and the octaethyltetraazaporphyrin methyl hydrogen resonance. (OETAP)-Rh–P(O)(OCH_3)$_2$: ^1H NMR (C_6D_6) δ = 4.02 (m, 16H, $-CH_2$), 1.95 (t, 24H, $-CH_3$), 0.96 (d, 6H, P(O)(OCH_3)$_2$), J_{P-H} = 12.0 Hz; FAB MS m/e 748 (calculated for (OETAP)Rh–P(O)(OCH_3)$_2$ m/e = 748). (OETAP)Rh(CH_3)($P(OCH_3)_3$): ^1H NMR (C_6D_6) δ = 4.00 (m, 16H, $-CH_2-$), 1.94 (t, 24H, $-CH_3$), –6.63 (d, 3H, Rh–CH_3), J_{Rh-H} = 2.3 Hz.

$H_2C{=}CH_2$. Vacuum-adapted NMR tubes containing C_6D_6 solutions of $[(OETAP)Rh]_2$ (1 mg/0.5 mL) were pressurized with ethene or [^{13}C]-ethene (200–700 Torr) and sealed. The NMR tubes were protected from light, and ^1H NMR was utilized in following the reaction progress at 295 K. (OETAP)Rh–CH_2CH_2–Rh(OETAP) has relatively low solubility in benzene, which resulted in a portion of product precipitating. A period of 1 month was required for the reaction to achieve equilibrium at 295 K. Integration of the ^1H NMR solutions that achieved equilibrium was used in evaluating the equilibrium constant (K_5 = [7]/[1]-[$CH_2{=}CH_2$]) at 295 K. The average value obtained for K_5(295 K) from three independent samples was 130 ± 30 (K_5(295 K) = 130 ± 30; $\Delta G_5°$(298 K) = –2.9 ± 0.1). (OETAP)Rh–CH_2CH_2–Rh(OETAP): ^1H NMR (C_6D_6) δ = 3.71 (m, 32H, $-CH_2-$), 1.83 (t, 48H, $-CH_3$), –10.57 (s, 4H, $-CH_2CH_2-$), $J_{^{13}C-H}$ = 142.6 Hz.

Pyridine. Solutions resulting from dissolution of $[(OETAP)Rh]_2$ in pyridine were prepared for spectroscopic studies by vacuum-transfer of pyridine into NMR, EPR, and electronic spectral cells containing $[(OETAP)Rh]_2$. The parent ion in the FAB MS for the species present in pyridine-d_5 solution occurs at m/e = 807, which is compatible with the molecular formula (OETAP)Rh(NC_5D_5)$_2$ (m/e = 807). ^1H NMR shifts for the CH_2 and CH_3 hydrogens manifest an inverse temperature dependence associated with Curie paramagnetic behavior (^1H NMR (NC_5D_5, T = 295 K) δ 28.8 (br, 16H, $-CH_2-$), 0.91 (br, 24H, $-CH_3$)). Frozen pyridine solutions (90 K) display a broad EPR signal centered at g = 1.998, characteristic of a ligand-based radical. The UV–visible spectrum in pyridine has a broad low energy peak (λ = 750 nm), which is indicative of a π radical (UV–vis (NC_5H_5) λ_{max} = 397, 470, 500, 576, 605, 750 nm). Dissolution of **1** in NC_5H_5, removal of excess NC_5H_5 under vacuum to produce a powder sample, and then transferring C_6D_6 as solvent resulted in observing the reappearance of the electronic spectrum for **1** and an ^1H NMR for **1** and NC_5H_5. Integration of the ^1H NMR yielded 3.8 ± 0.2 for the molar ratio of NC_5H_5 to **1**.

High-Temperature NMR Studies. ^1H NMR studies in C_6D_6 at elevated temperatures were carried out in medium- and thick-walled NMR tubes (Wilmad) sealed below the spinner such that the entire solution was thermostated. Sealing the sample tubes was accomplished by fixing the top and bottom so they remained concentric and collapsing the walls of the tube containing the frozen sample solution. The tube was sealed at a position where the sample was confined below the spinner, which minimized thermal gradients in the sample.

The choice of NMR tube thickness was determined by the vapor pressure of the solvent at the highest temperatures to be studied. In the specific case of benzene solvent ($\Delta H°_{vap}$(353 K) = 7.36 kcal mol^{-1}, $\Delta S°$ = 20.8 cal K^{-1} mol^{-1}), the vapor pressure at 150 °C(423 K) is ~5.5 atm, so that a medium-wall NMR tube was adequate if the tube was properly sealed. Each sample was tested behind a shock shield at high temperatures prior to doing NMR experiments to ensure that the sealed tube could sustain the elevated pressures.

X-ray Structure Determination. Deep purple crystals of (OETAP)-Rh–CH_3 were obtained by slow evaporation of solvent from a chloroform/ethanol solution at room temperature. (Octaethyltetraazaporphyrinato)-rhodium(III) methyl, $RhN_8C_{33}H_{43}$, crystallized in the monoclinic space group $P2_1/c$ (systematic absences: $h0l$, l = odd; $0k0$, k = odd) with a = 9.889(2) Å, b = 22.660(4) Å, c = 14.781(3) Å, β = 106.85(2)°, V = 3170(2) Å^3, Z = 4, and d_{calc} = 1.372 g/cm^3. The cell constants were determined from a least-squares fit of the setting angles for 25 accurately centered reflections. X-ray intensity data were collected at room temperature (295 K) on an Enraf-Nonius CAD4 diffractometer employing graphite-monochromated Cu Kα radiation (λ = 1.541 84 Å) and using the ω–2θ scan technique. A total of 5568 reflections were measured over the following ranges: $4 \le 2\theta \le 130°$, $0 \le h \le 12$, $0 \le k \le 27$, $-18 \le l \le 18$. Three standard reflections measured every 3500 s of X-ray exposure showed no intensity decay over the course of data collection.

The intensity data were corrected for Lorentz and polarization effects, and an empirical absorption correction was applied. Of the reflections measured, a total of 4234 unique reflections with $F^2 > 3\sigma(F^2)$ were used during subsequent structure refinement.

The structure was solved by standard heavy-atom Patterson methods followed by weighted Fourier syntheses. Refinement was performed by full-matrix least-squares techniques based on F to minimize the quantity $\sum w(|F_o| - |F_c|)^2$ with $w = 1/(\sigma^2 + 0.02F_o^2 + 2.0)$. Non-hydrogen atoms were refined anisotropically, and hydrogen atoms were included as constant contributions to the structure factors and were not refined. Refinement converged to R_1 = 0.049 and R_2 = 0.055.

Acknowledgment. We gratefully acknowledge support of this work by the National Science Foundation (Grant CHE90-14923) and the Department of Energy, Division of Chemical Sciences, Offices of Basic Energy Sciences, (Grant DE-FG02-86ER13615). J.P.F. gratefully acknowledges support from the Petroleum Research Fund, administered by the American Chemical Society, from the Army Research Office, and from the Naval Academy Research Council.

Supplementary Material Available: A Line drawing of (OETAP)-Rh–CH_3 as well as tables of crystallographic data, refined hydrogen positional parameters, refined thermal parameters, bond distances, and bond angles (6 pages). Ordering information is given on any current masthead pages.